GMR
The Original

ECO-FRIENDLY SYNTHESIS OF NICKEL NANOPARTICLES FROM OCIMUM SANCTUM: ANTIBACTERIAL AND PHOTOCATALYTIC ACTIVITY

Jaydeep V. Deore*[1, 4], Bhushan B. Khiarnar[2], Rajashri B. Savant[1,3]

[1]Department of Chemistry, M.S.G. Arts, Science and Commerce College Malegaon, Maharashtra, India
[2]Interdisciplinary School of Science (IDSS), Savitribai Phule Pune University, Ganeshkhind, Pune 411007, India
[3]Department of Chemistry, M.P.H. Arts, Science and Commerce Mahila Mahavidyalay Malegaon, Maharashtra, India
[4]Department of Chemistry, G. M. Vedak College of Science, Tala-Raigad, 402111, Maharashtra, India
*Corresponding author. E-mail address: rajashrib.savant@gmail.com

GRAPHICAL ABSTRACT

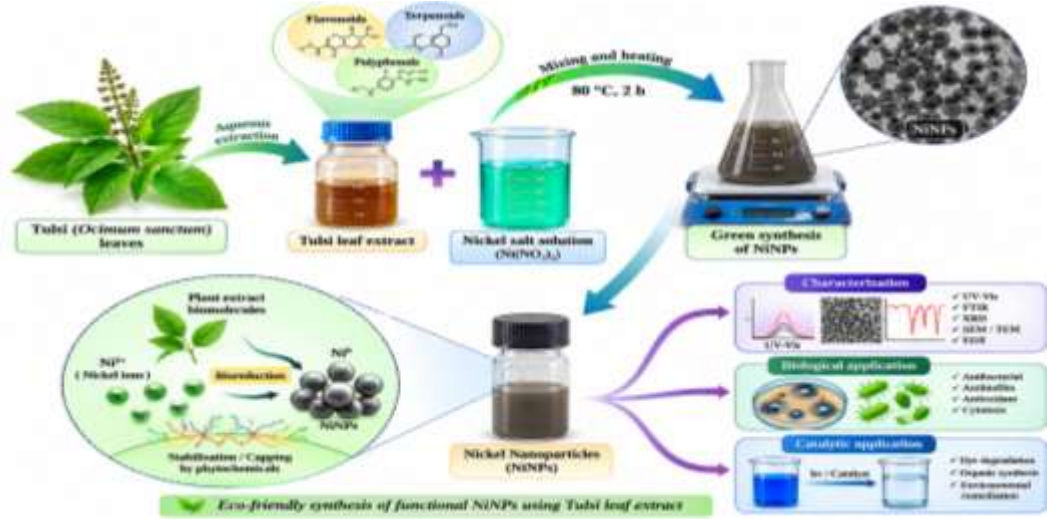

ABSTRACT

Green synthesis of metallic nanoparticles offers a sustainable alternative to conventional chemical approaches. In this study, nickel nanoparticles (NiNPs) were successfully produced with Ocimum sanctum (Tulsi) leaf extract, which served as both a natural reducing and capping agent. Characterization involved UV–Vis spectroscopy at 387 nm, Fourier-transform infrared (FTIR) spectroscopy, XRD analysis, scanning electron microscopy (SEM), and energy-dispersive X-ray spectroscopy (EDS). XRD confirmed the face-centered cubic (FCC) crystalline structure of the biogenic NiNPs, whose sizes ranged from 18-20 nm. The findings also showed that the particles were crystalline and predominantly spherical, while indicating the contribution of plant phytochemicals to their synthesis and stabilization. Biological testing found notable antibacterial activity against the target bacterial strains, as well as radical-scavenging capacity in DPPH assays. The synthesized NiNPs also efficiently degraded methylene blue, an organic dye pollutant, under light irradiation. These results point to the potential of O. sanctum-mediated NiNPs as eco-friendly nanomaterials for environmental and biological applications.

KEYWORDS: Green synthesis, nickel nanoparticles, antibacterial activity, photocatalytic degradation

1. INTRODUCTION

Nanotechnology allows material properties to be controlled precisely through adjustments to particle size and shape, as well as surface structure, defects, and chemical composition. Together, these features determine optical, magnetic, catalytic, and biological behavior, supporting applications in sensing, energy conversion, medicine, and environmental remediation [1–3]. Conventional physical and chemical approaches provide considerable control over nanoparticle formation but may require toxic reducing or stabilizing agents, organic solvents, elevated temperatures or pressures, and substantial energy input. These limitations can increase production costs and generate chemical waste. Consequently, plant-mediated synthesis has emerged as an attractive alternative for producing nanoparticles under comparatively mild conditions. Plant extracts contain phytochemicals, including phenolic compounds, flavonoids, terpenoids, proteins, carbohydrates, and other secondary metabolites, which can participate in metal-ion reduction, complexation, nucleation, growth, and surface stabilization [4–6]. The properties of the resulting nanoparticles are strongly influenced by the plant

species and extract composition, as well as extraction conditions, pH, precursor concentration, reaction temperature, and reaction time.

Nickel-based nanomaterials (Ni-based NPs) have received growing attention for environmental and catalytic applications because of their high surface reactivity, redox properties, and potential photocatalytic activity. Ni-based NPs are mainly found as metallic Ni, NiO, or mixed Ni/NiO phases. Their physicochemical properties and overall performance depend strongly on factors such as phase composition, oxidation state, crystallinity, particle size, morphology, surface chemistry, and structural defects [7–9]. These characteristics make Ni-based NPs promising for applications in sensing, catalysis, photocatalysis, energy storage, adsorption, and antimicrobial systems. Compared with noble-metal NPs, Ni-based NPs offer lower cost and greater elemental abundance, providing attractive alternatives for applications requiring magnetic, redox, catalytic, electrochemical, or semiconducting properties [10–12].

Biological activity has also been reported for green-synthesized nickel-based nanomaterials produced with extracts from a range of other plants, Rhamnus virgata [13], Punica granatum juice [14], Abutilon indicum [15], Paulownia tomentosa [16], and Aegle marmelos [17,18] has described antibacterial, antioxidant, cytotoxic, and other related biological activities. Mirza et al. [19] reported a biogenic synthesis of nickel-based NPs using Toona ciliata, Ficus carica and Pinus roxburghii for their biological applications.

The antibacterial activity of NiNPs has been associated with reactive oxygen species generation, membrane disruption, increased permeability, intracellular leakage, and nickel-ion release [20-23]. These effects are influenced by particle size, morphology, surface characteristics, concentration, and surrounding medium [24-28]. Despite these advances, comparatively few studies have systematically integrated the synthesis, comprehensive characterization, and antibacterial evaluation of O. sanctum (Tulsi)-mediated NiNPs. In this study, nickel nanoparticles (NiNPs) were produced through a green synthesis method using O. sanctum leaf extract as a natural reducing and stabilizing agent. This botanical extract offers a straightforward, environmentally friendly alternative to conventional chemical synthesis, reducing the need for harsh reaction conditions and harmful compounds [29-33]. The synthesized NiNPs were characterized with suitable physicochemical techniques to examine their structural, morphological, and elemental properties. Their potential in practical applications was then assessed by measuring antibacterial efficacy. The findings indicate that NiNPs derived from O. sanctum may serve as eco-friendly agents in antibacterial and environmental applications.

2. MATERIALS AND METHODS

2.1 Materials

Nickel nitrate [Ni (NO3)2], analytical grade was purchased from SRL Chem, India. Deionized (DI) water and analytical-grade ethanol were used throughout the study. Fresh Ocimum sanctum (Tulsi) leaves were collected from the campus of G. M. Vedak College of Science, Tala–Raigad, Maharashtra, India.

2.2 Preparation of Ocimum sanctum Leaf Extract

The freshly collected O. sanctum leaves were thoroughly rinsed with running tap water to remove adhering dust, dirt, and other surface contaminants. After that, they were repeatedly cleaned with double-distilled water and allowed to air dry for 48 hours in the shade until there was no more surface moisture. A 250 mL Erlenmeyer flask with 100 mL of double-distilled water was filled with 20 g of finely chopped leaf material after it had dried. To extract soluble phytochemicals, the mixture was heated to 65°C for 30 minutes while being constantly agitated with a magnetic stirrer [34]. The dark green aqueous extract was filtered through muslin cloth and Whatman No. 1 filter paper (11 µm pore size) once it had cooled to room temperature. The resultant clear filtrate was kept in an airtight amber glass container at 4°C until nanoparticle synthesis.

2.3 Green Synthesis of Nickel Nanoparticles (NiNPs)

To synthesize NiNPs, 30 mL of freshly prepared O. sanctum was added to 70 mL of a 5 mM $Ni(NO_3)_2 \cdot 6H_2O$ precursor solution. The mixture was vigorously stirred at 800 rpm with a magnetic stirrer and heated at 80°C for 2 hours. Its pH was adjusted to 9 using 1 M NaOH. Bio-reduction and Ni NP formation were confirmed by the color shift from light green to dark brown [35]. Afterward, the colloidal suspension was centrifuged at 5,000 rpm for 15 minutes. The precipitate was washed three times with double-distilled water and twice with absolute ethanol to remove unreacted nickel ions and unbound phytochemical residues. The purified material was collected and left at room temperature for 12 h.

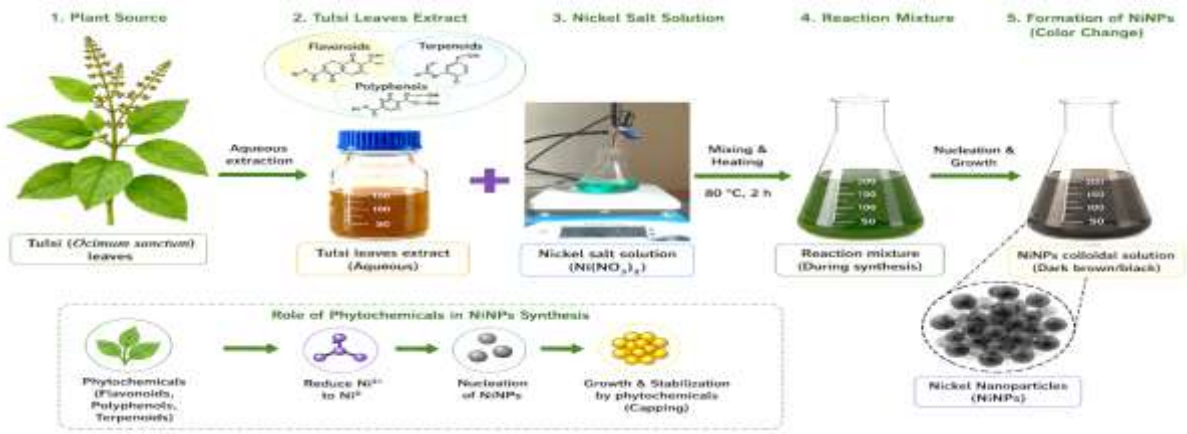

Figure 1. Green Synthesis of Nickel Nanoparticles (NiNPs) Using O. sanctum Leaf Extract

2.4 Physicochemical Characterization Techniques

2.4.1 UV–Visible Spectroscopy

The formation of biogenic nickel nanoparticles (NiNPs) was confirmed through UV–Visible spectroscopy with a Shimadzu UV-1900i double-beam UV–Visible spectrophotometer, scanning wavelengths from 200–800 nm. Recording the absorption spectrum made it possible to examine the characteristic optical response of the synthesized NiNPs and obtain preliminary evidence that nanoparticles had formed 36]. The spectral profile also helped assess how the nanoparticles interacted with phytochemicals in the plant extract.

2.4.2 Fourier Transform Infrared (FTIR) Spectroscopy

Fourier-transform infrared (FTIR) spectroscopy was carried out to investigate the biomolecular functional groups responsible for the bio-reduction of Ni^{2+} ions and the subsequent stabilization of the synthesized NiNPs. FTIR spectra of the O. sanctum leaf extract and the dried NiNPs were acquired using a PerkinElmer Spectrum Two FTIR spectrometer in the 4000–400 cm^{-1} wavenumber region. Samples were prepared using the potassium bromide (KBr) pellet method to facilitate the identification of phytochemical constituents participating in nanoparticle formation and surface capping

2.4.3 X-Ray Diffraction (XRD) Analysis

The crystal structure and phase purity of the biosynthesized nickel nanoparticles (NiNPs) were investigated using a X-ray diffractometer equipped with Cu-Kα radiation (λ = 1.5406 Å), operated at 40 kV and 40 mA. X-ray diffraction (XRD) patterns were recorded over a 2θ range of 20–80° at room temperature. The average crystallite size (D) was estimated from the broadening of the most intense diffraction peaks using the Debye–Scherrer equation:

$$D = \frac{0.9\lambda}{\beta\cos\theta}$$

Where, D is the average crystallite size, λ is the wavelength of the incident X-ray (1.5406 Å),
β is the full width at half maximum (FWHM) of the diffraction peak expressed in radians, θ is the corresponding Bragg angle.

2.4.4 SEM–EDS Characterization

The surface morphology of the biosynthesized NiNPs was examined using a Thermo Scientific Scios 2 scanning electron microscope (SEM). Elemental composition was determined by energy-dispersive X-ray spectroscopy (EDS) and operated at an accelerating voltage of 20 kV. SEM–EDS analysis was used to evaluate the morphology and elemental composition of the synthesized nanoparticles, as this combined approach provides complementary information on nanoparticle morphology and elemental composition [37].

2.4.5 TEM Characterization

The morphology and particle size of the green-synthesized NiNPs were further investigated using an FEI Tecnai TF20 high-resolution transmission electron microscope operated at 200 k. The TEM analysis was performed to determine the particle morphology, size distribution, dispersion, and structural characteristics of the synthesized NiNPs. TEM is widely used for nanoscale morphological and structural characterization, while high-resolution imaging can provide detailed information on particle dimensions and internal structure [38].

2.5 Biological and Environmental Application Assays

2.5.1 Antibacterial Assay

The antibacterial activity of the biosynthesized nickel nanoparticles (NiNPs) was evaluated against Gram-negative Escherichia coli (ATCC 25922) and Gram-positive Staphylococcus aureus (ATCC 25923) using the agar well diffusion assay [39]. Fresh bacterial cultures were adjusted to the 0.5 M6cFarland turbidity standard (approximately 1.5×10^8 CFU/mL from Mueller-Hinton Broth) and uniformly spread onto Muller-Hinton Agar (MHA) plates was loaded with solvent alone which served as vehicle control and Ciprofloxacin disc (8µg) was taken as positive control. Subsequently, 50 µL of NiNP suspensions at concentrations of 25, 50, 75, and 100 µg/mL were dispensed into the respective wells. The inoculated plates were incubated at 37 °C for 24 h, after which the antibacterial activity was determined by measuring the diameter of the inhibition zones (ZOI, mm) [40-43]. All experiments were performed in triplicate

2.5.2 Antioxidant DPPH Radical Scavenging Assay

The free radical scavenging capacity of NiNPs was evaluated using the 2,2-diphenyl-1-picrylhydrazyl (DPPH) assay [44]. A freshly prepared DPPH solution (0.1 mM in methanol) was mixed with 1 mL of NiNPs suspensions at concentrations ranging from 1 to 1000 µM. The reaction mixtures were incubated in the dark at room temperature for 30 minutes. Absorbance was recorded at λ = 517 nm against a methanol blank. L-ascorbic acid was used as the standard antioxidant reference. The radical scavenging activity (%) was calculated as:

$$\%RSA = \frac{Abs_{(Control)} - Abs_{(Sample)}}{Abs_{(Control)}} x\ 100$$

Where, RSA = Radical Scavenging Activity, Abs (Control) = Absorbance of control and
Abs (Sample) = Absorbance of sample

2.5.3 Photocatalytic Dye Degradation

The photocatalytic activity of NiNPs was investigated by monitoring the degradation of Methylene Blue (MB) dye in an aqueous system under UV light irradiation [45-47]. In a typical experiment, 50 mg of NiNPs was suspended in 100 mL of an aqueous MB dye solution (10 mg/L). The suspension was stirred in the dark for 30 minutes to establish adsorption–desorption equilibrium between the dye and nanoparticle surface, consistent with earlier photocatalytic MB studies. The mixture was then exposed to light under continuous agitation. At 20-minute intervals over a 120-minute reaction period, 3 mL aliquots were collected, centrifuged to remove catalyst particles, and analysed by recording the absorbance at λmax = 664 nm, as commonly applied in MB degradation experiments. The dye degradation percentage was determined using:

$$\text{Degradation Efficiency (\%)} = \frac{C_0 - C_t}{C_0} x\ 100$$

3. RESULTS AND DISCUSSION

3.1 UV–Visible Spectroscopic Analysis

The formation of NiNPs was first monitored using UV–Visible spectroscopy. After O. sanctum leaf extract was reacted with nickel nitrate, the mixture gradually turned from pale green to dark brown, suggesting the formation of nickel-based nanoparticles. A distinct absorption maximum appeared at 386 nm (Figure 2) in the UV–Visible spectrum. For NiNPs synthesized with O. sanctum leaf extract, Pandian et al. [48] reported a maximum at 395 nm, closely matching the present observation. Differences in particle size, surface chemistry, precursor concentration, and reaction conditions may account for the slight shift. Thus, the absorption band at 389 nm offers preliminary spectroscopic evidence of NiNP formation, with further support from the XRD, FTIR, SEM–EDS, and TEM analyses.

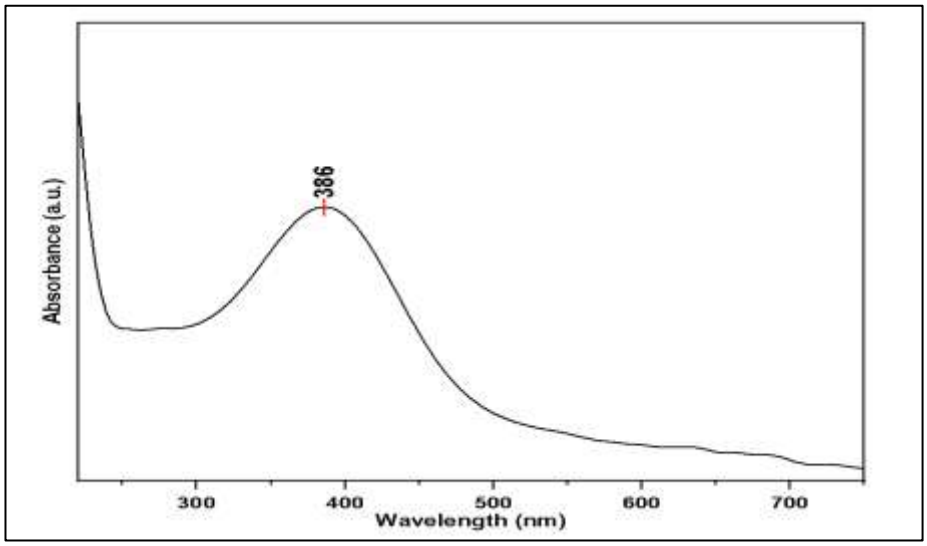

Figure 2. UV-DRS absorbance spectra of green synthesized Ni NPs.

3.2 FTIR Analysis: Bio-reduction and Surface Capping

The FTIR spectrum of the green-synthesized NiNPs displayed several characteristic bands (Figure 3). Those at 3479.01 and 3169.23 cm^{-1} corresponded to O–H/N–H stretching, pointing to hydroxyl- and amino-containing phytochemicals. Plant-mediated NiNPs have likewise been reported to show O–H/N–H, aromatic, C–N, and C–O vibrations, supporting the participation of plant biomolecules in nanoparticle formation and stabilization [48,49]. In related work, Pandian et al. synthesized NiNPs with O. sanctum leaf extract, and Elango et al. used FTIR analysis to confirm phytochemical functional groups associated with biosynthesized NiNPs [48,49]. For Fumaria officinalis-mediated NiNPs, Huang et al. observed comparable organic functional groups along with Ni–O vibrations [50]. Kumar et al. also demonstrated that plant biomolecules may serve as reducing, capping, and stabilizing agents during NiNP synthesis [51]. In this study, the bands observed at 1596.87, 1350.46, and 1040.68 cm^{-1} were attributed to C=C/C=N, C–N/C–H, and C–O vibrations, respectively. The band at 599.48 cm^{-1} may be associated with Ni–O or other metal–oxygen vibrations [50]. Taken together, the FTIR findings suggest that phytochemicals from O. sanctum remained attached to the NiNP surface, contributing to both their formation and stabilization [48–51].

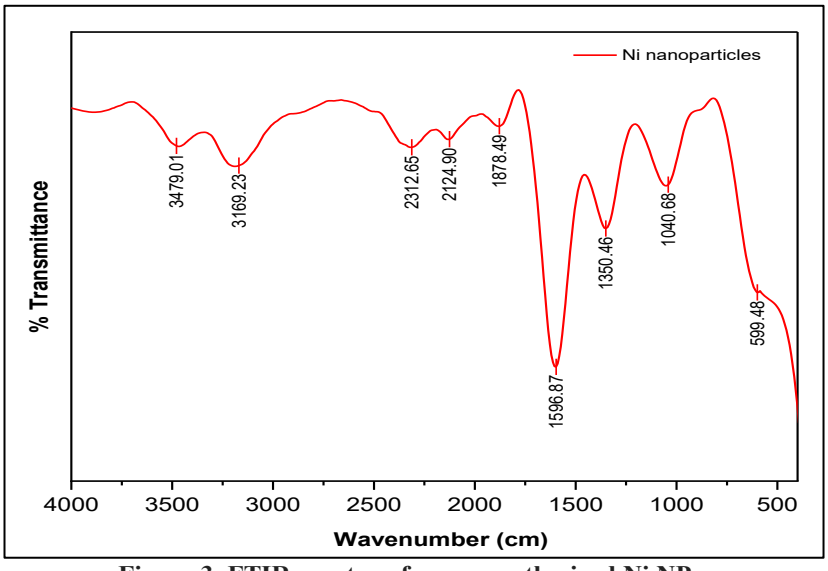

Figure 3. FTIR spectra of green synthesized Ni NPs.

3.3. X-ray Diffraction (XRD) Analysis

The synthesized NiNPs were examined by X-ray diffraction (XRD), with the resulting diffractogram presented in Figure 4. Three clear reflections appeared at 2θ = 44.34°, 51.66°, and 76.22°. These were assigned to the (111), (200), and (220) planes, respectively, of face-centered cubic (fcc) metallic Ni. Their positions agree with the characteristic fcc-Ni peaks reported at approximately 44.5°, 51.8°, and 76.4°, as well as with PDF No. 04-0850 [52–54]. The reflections are sharp and well defined, indicating that the synthesized NiNPs have good crystallinity. Within the detection limit of the XRD analysis, no additional distinct reflections associated with crystalline NiO or other secondary phases were observed, suggesting that the sample predominantly consists of metallic Ni. Comparable XRD patterns, marked by characteristic fcc-Ni reflections and no detectable crystalline oxide phases, have been reported previously [52–54]. Taken together, these results indicate that the adopted green-synthesis approach produced predominantly crystalline fcc metallic Ni nanoparticles.

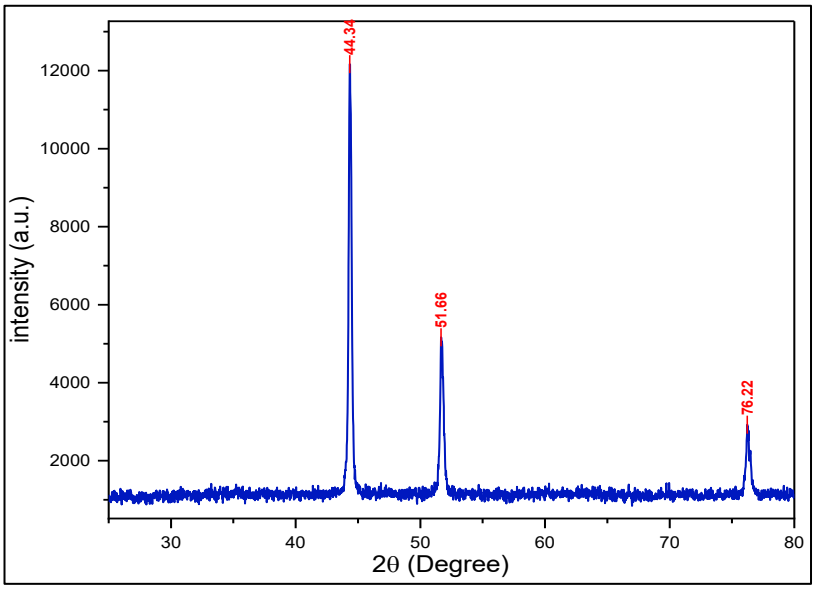

Figure 4 XRD pattern of O. sanctum leaf extract bio fabricated NiNPs

The average crystallite size was calculated using the Debye–Scherrer equation:

$$D = \frac{K\lambda}{\beta \cos\theta}$$

where D is the crystallite size, λ is the X-ray wavelength, β is the full width at half maximum (FWHM), and θ is the Bragg diffraction angle.

3.4. SEM–EDS Surface Topography and Elemental Profile

3.4.1 SEM–EDS Surface Morphology and Elemental Composition

The morphology and elemental composition of the biosynthesized NiNPs were examined using SEM coupled with EDS. Most particles appeared spherical or nearly spherical in the SEM images, although some aggregation was also visible (Figure 5a-b). Comparable morphologies have been described for plant-mediated NiNPs, and the observed aggregation may result from interparticle interactions and phytochemicals bound to the particle surfaces. Nearly spherical NiNPs synthesized with O. sanctum leaf extract was reported by Pandian et al. [48]. Yuan et al. observed spherical NiNPs produced using Alhagi maurorum leaf extract [55], and Huang et al. likewise reported spherical NiNPs prepared with Fumaria officinalis extract [50]. In the present study, the EDS spectrum displayed a strong Ni signal, confirming that nickel was the major elemental component of the synthesized material (Figure 5c). Comparable SEM–EDS characterization has helped determine the morphology and elemental composition of plant-mediated NiNPs. Taken together, these findings indicate that NiNPs formed successfully, were predominantly spherical, and consisted primarily of nickel.

3.4.2 TEM Analysis

TEM analysis provided further confirmation of the morphology and particle-size distribution of the synthesized NiNPs. In Figure 5(d–f), the particles appear predominantly spherical or quasi-spherical, with a fairly uniform distribution and only limited aggregation. According to the particle-size histogram in Figure 5f, their average size was 19.6 ± 0.5 nm, confirming that the synthesized NiNPs were nanoscale. This value is comparable to those reported for NiNPs produced through plant-mediated methods. Using O. sanctum leaf extract, Pandian et al. obtained almost spherical NiNPs measuring 12–36 nm [48]. Elango et al. likewise confirmed the formation of nanosized NiNPs, with an average particle size of about 47 nm, though the particles had a different morphology [49]. In a more recent study, Kumar et al. reported plant-mediated NiNPs ranging from 7–18 nm and showed that plant biomolecules contribute to their reduction, capping, and stabilization [51]. The review by Kondak et al. further underscored the value of phytochemicals and complementary microscopic methods for understanding the formation and physicochemical properties of green-synthesized NiNPs [56]. Taken together, the SEM–EDS and TEM findings verify the nanoscale character and mainly spherical shape of the synthesized NiNPs, while also supporting the role of O. sanctum phytochemicals in their formation and stabilization.

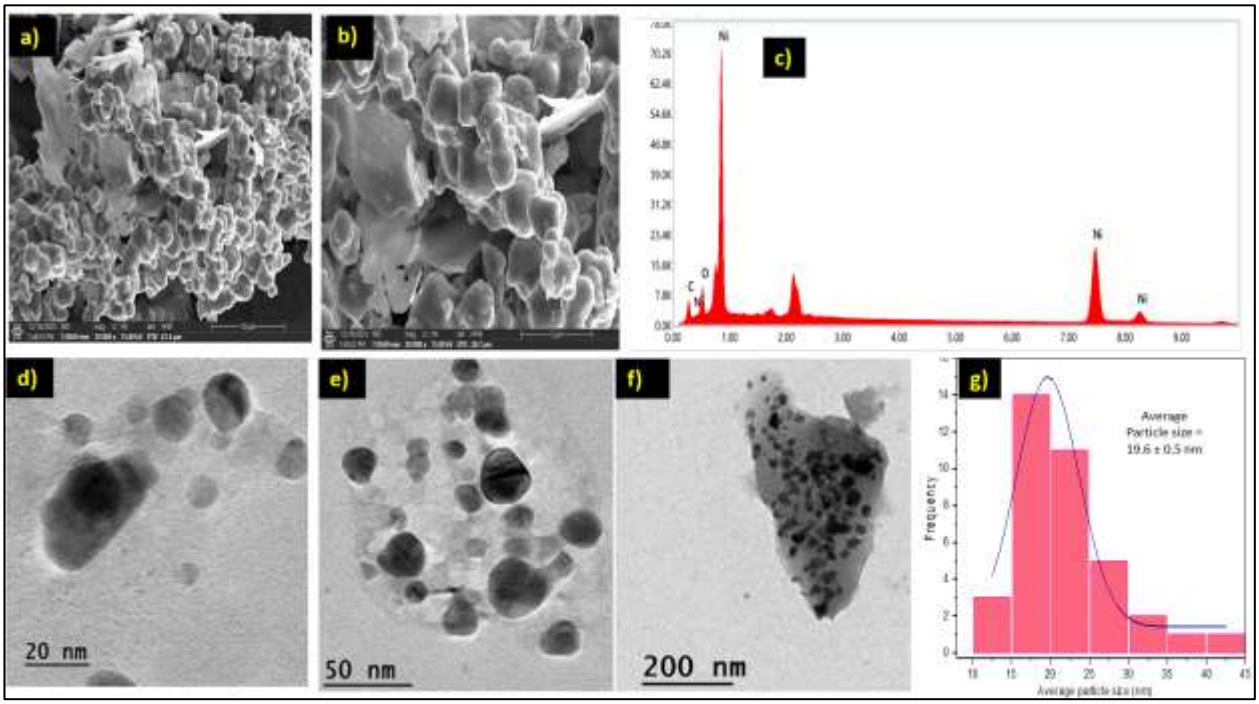

Figure 5. Characterization of green-synthesized nickel nanoparticles (NiNPs): (a,b) FE-SEM images, (c) EDX spectrum, (d–f) TEM micrographs, and (g) TEM-derived particle size distribution.

3.5. Biological Evaluation: Antibacterial and Radical Scavenging Efficacy

3.5.1 Antibacterial

The antibacterial activity of the biosynthesized NiNPs was tested against the Gram-negative bacteria Escherichia coli (ATCC 25922) and Pseudomonas aeruginosa (ATCC 27853). Table 1 shows that inhibition increased as the NiNP concentration rose. This concentration-dependent effect agrees with earlier reports on plant-mediated nickel-based nanoparticles [57,58]. In particular, recent studies have found significant antimicrobial activity from plant-mediated NiNPs against pathogenic bacteria, indicating that biologically synthesized NiNPs may serve as antimicrobial materials [57]. Green-synthesized nickel-based nanoparticles have also inhibited both E. coli and P. aeruginosa to measurable degrees, though the response depends on the bacterial strain and the characteristics of the nanoparticles [58]. Fresh bacterial cultures were adjusted to a 0.5 McFarland turbidity standard, approximately 1.5×10^8 CFU mL^{-1}, in accordance with standardized antimicrobial susceptibility-testing recommendations [59]. They were then spread evenly across Mueller–Hinton agar plates with sterile cotton swabs. Using a cork borer, sterile 6-mm wells were made in the agar, and 50 µL of NiNP suspension at 25, 50, and 100 µg mL^{-1} was placed into the corresponding wells. Ciprofloxacin (8 µg disc) served as the positive control; sterile distilled water was the negative control. Following incubation at 37 °C for 24 h, antibacterial activity was assessed by measuring the inhibition-zone diameter (mm). Each experiment was conducted in triplicate, with results reported as mean ± standard deviation (SD).

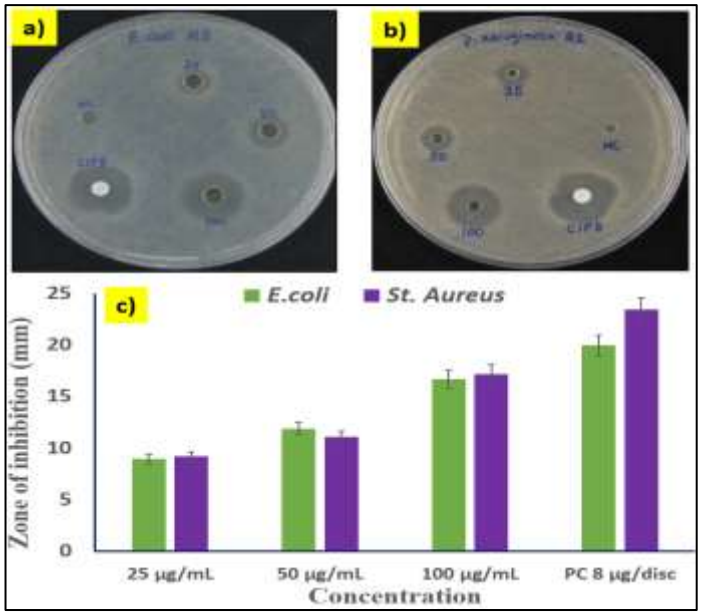

Figure 6. Antibacterial activity of Ni NPs against a) Gram-negative E. coli, b) Gram-positive St. aureus evaluated by agar well diffusion assay and c) mean zone of inhibition (mm) with SD error bars (n = 3)

3.5.2 Antioxidant DPPH Radical Scavenging Assay

The DPPH radical-scavenging assay was used to assess the antioxidant activity of the green-synthesized NiNPs [59]. As the NiNP concentration rose, DPPH inhibition increased from 1.63% at 1 µM to 73.46% at 1000 µM. The standard was more active, reaching 82.26% at 50 µM (Table 1), as shown in Figure 7. This activity may be associated with phytochemicals from O. sanctum attached to the NiNP surface. Phenolic and flavonoid compounds may scavenge radicals through hydrogen-atom and electron-transfer mechanisms [60,61]. Comparable concentration-dependent antioxidant effects have been described for nickel nanoparticles produced with plants. Fumaria officinalis -mediated NiNPs, for instance, had a DPPH IC_{50} of 145 µg/mL, whereas Rhamnus virgata -mediated NiO nanoparticles showed 70.36% DPPH scavenging activity. More recently, NiNPs mediated by Shorea robusta showed concentration-dependent DPPH scavenging activity, reaching 84.3% at the highest concentration tested. Taken together, these findings support the antioxidant potential of plant-mediated nickel-based nanoparticles, while the O. sanctum-mediated NiNPs showed a clear concentration-dependent response in radical scavenging.

Table1: Comparative RSC % Inhibition of Ni NPs and Standard

Ni Nanoparticles		Standard	
Concentration (µM)	**RSC % Inhibition**	**Concentration (µM)**	**RSC % Inhibition**
1	1.63	0.78	2.15
10	2.10	1.56	6.67
50	10.77	3.125	19.30
100	31.40	6.25	36.38
250	45.43	12.5	61.47
500	68.05	25	75.03
1000	73.46	50	82.26

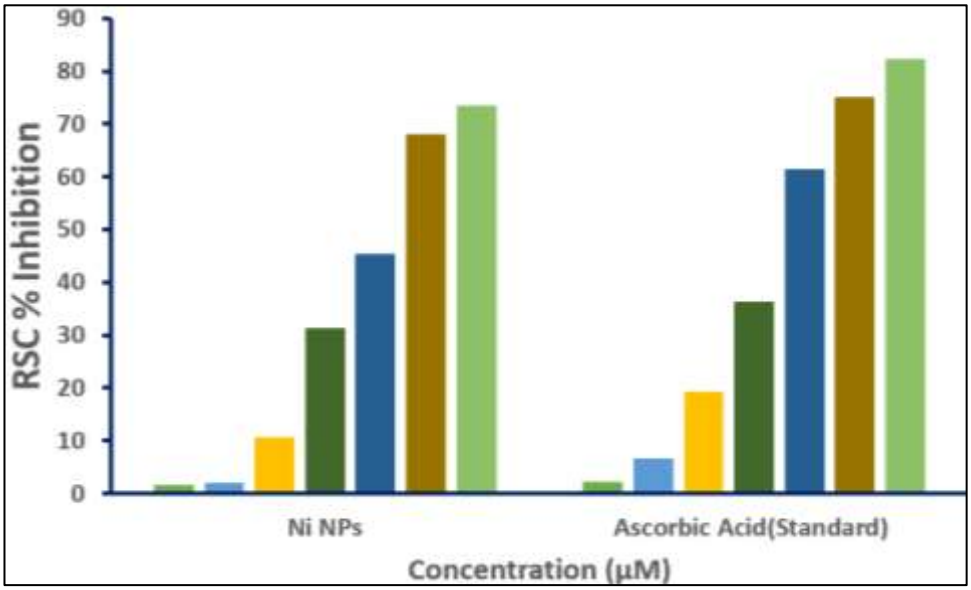

Figure 7. DPPH radical scavenging activity of Ni NPs (n = 3).

3.6 Photocatalytic Dye Degradation and Mechanism

The photocatalytic activity of the green-synthesized nickel nanoparticles (NiNPs), produced with O. sanctum leaf extract, was assessed using methylene blue (MB) as a model organic dye. As irradiation continued, MB's characteristic absorption band at approximately 664 nm gradually declined, showing that the dye concentration was steadily decreasing (Figure 8a). Under the conditions investigated here, MB degradation rose with irradiation time and reached approximately 78% after 120 min. Previous studies have likewise shown that Ni-based nanoparticles can promote MB degradation/reduction, with the reaction potentially following pseudo-first-order kinetics [58-60]. The kinetic data were fitted using the pseudo-first-order equation: $\ln\frac{C_0}{C_t} = k_{obs}.t$

where C0 and Ct represent the initial and residual MB concentrations, respectively, and is the apparent rate constant.

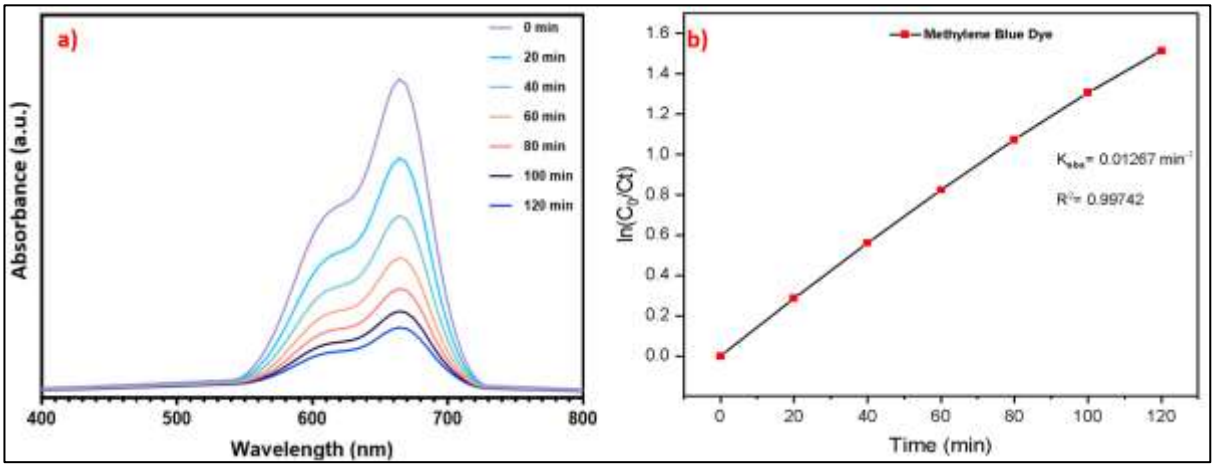

Figure 9. Photocatalytic degradation of methylene blue by green-synthesized NiNPs: (a) UV–Vis spectra and (b) pseudo-first-order kinetics

The corresponding plot (Figure 8(b)) displayed a highly linear relationship, yielding an apparent rate constant of 0.01267 min^{-1} and an value of 0.99742. This strong correlation suggests that MB degradation followed pseudo-first-order kinetics under the conditions employed [61,62]. The photocatalytic activity may also depend on the surface characteristics of the NiNPs, as well as on phytochemicals from the O. sanctum leaf extract that may contribute to nanoparticle formation and surface stabilization. Taken together, the results indicate that the green-synthesized NiNPs show good potential for removing MB photocatalytically from aqueous systems.

Proposed degradation mechanism

NiNPs + hν → Ni(e^- + h+)

Ni(e-) + O2 → •O2-

Ni(h+) + H2O/OH^- → •OH

MB + •O2-/•OH→ degradation products

The generated reactive oxygen species (•O2- and •OH) attack the MB molecules and convert them into smaller degradation products (Figure 9).

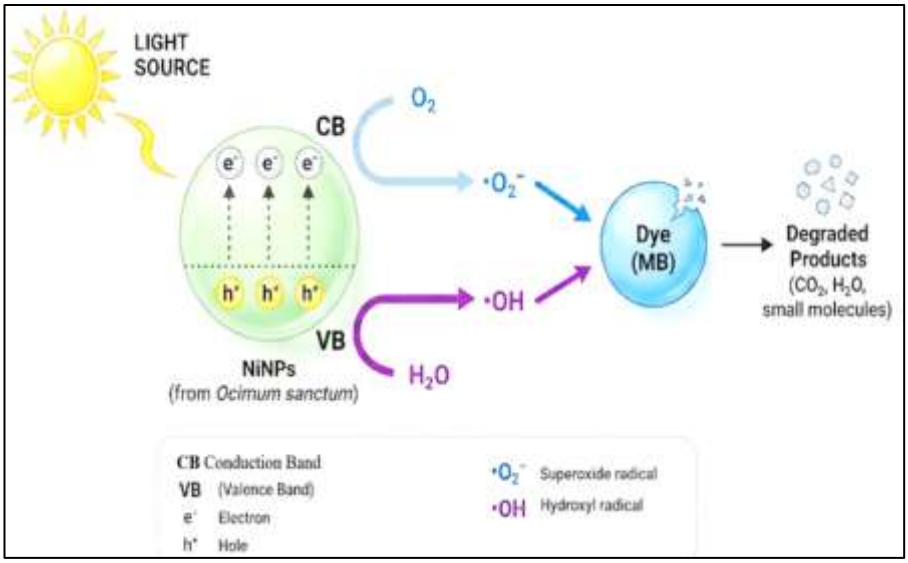

Figure 9. Proposed photocatalytic degradation mechanism of methylene blue using Oncium sanctum mediated Ni NPs

4. CONCLUSION

The present study demonstrates that Ocimum sanctum (Tulsi) leaf extract provides a simple and sustainable route for the synthesis of crystalline NiNPs. UV–Visible spectroscopy showed an absorption maximum at 389 nm, while FTIR confirmed the involvement of plant-derived functional groups in nanoparticle formation and stabilization. XRD revealed the characteristic (111), (200), and (220) reflections of face-centered cubic metallic Ni, with a crystallite size of 18.5 nm. SEM–EDS and TEM further confirmed predominantly spherical to quasi-spherical nanoparticles with an average particle size of 19.6 ± 0.5 nm. The synthesized NiNPs showed promising antibacterial, antioxidant, and photocatalytic activities. At 100 µg/mL, inhibition zones of 16.70 mm against E. coli and 17.19 mm against S. aureus were observed. The nanoparticles exhibited DPPH radical-scavenging activity with an IC_{50} of 48.2 µg/mL and achieved 78.00% methylene blue degradation within 120 min following pseudo-first-order kinetics. Overall, these findings highlight the potential of O. sanctum-mediated NiNPs for antibacterial applications and dye-contaminated wastewater treatment. Further studies on scale-up, stability, environmental safety, and toxicity are needed to assess their practical applicability.

REFERENCES

1. Baig, N., Kammakakam, I., & Falath, W. (2021). Nanomaterials: a review of synthesis methods, properties, recent progress, and challenges. Materials Advances, 2(6), 1821–1871.
2. Santhosh, P. B., & Ulrih, N. P. (2013). Multifunctional mesoporous silica nanoparticles for biomedical applications. Microporous and Mesoporous Materials, 180, 281–292.
3. Khan, I., Saeed, K., & Khan, I. (2019). Nanoparticles: Properties, applications and toxicities. Arabian Journal of Chemistry, 12(7), 908–931.
4. Singh, J., Dutta, T., Kim, K. H., Rawat, M., Samddar, P., & Kumar, P. (2018). 'Green' synthesis of metals and their oxide nanoparticles: applications for environmental remediation. Journal of Nanobiotechnology, 16, 84.
5. Akhtar, M. S., Panwar, J., & Yun, Y. S. (2013). Biogenic synthesis of metallic nanoparticles by plant extracts. ACS Sustainable Chemistry & Engineering, 1(6), 591–602.
6. Marslin, G., Siram, K., Maqbool, Q., Selvakesavan, R. K., Kruszka, D., Kachlicki, P., & Franklin, G. (2018). Secondary metabolites in the green synthesis of metallic nanoparticles. Materials, 11(6), 940.
7. Bonomo, M. (2018). Synthesis and characterization of NiO nanoparticles: A review. Journal of Nanoparticle Research, 20, 222.
8. Fathy, M., Kashyout, A. E. H. B., & Bassyouni, M. (2020). Synthesis and characterization of nickel oxide nanoparticles and their catalytic activity. Journal of Materials Research and Technology, 9(3), 6062–6072.
9. Theologidis, I. G., et al. (2021). Nickel and nickel oxide nanoparticles: Synthesis, structural properties, and catalytic applications. Catalysts, 11(10), 1205.
10. Gawande, M. B., Goswami, A., Felpin, F. X., Asefa, T., Huang, X., Silva, R., Zou, X., Zboril, R., & Varma, R. S. (2016). Cu and Cu-based nanoparticles: Synthesis and applications in catalysis. Chemical Reviews, 116(6), 3722–3811.
11. Gong, M., & Dai, H. (2015). A mini review of NiFe-based materials as highly active electrocatalysts for water oxidation. Nano Research, 8(1), 23–39.
12. Rahdar, A., Aliahmad, M., & Samavati, A. (2015). Synthesis and characterization of NiO nanoparticles: Magnetic and optical properties. Journal of Nanostructure in Chemistry, 5, 145–151.
13. Iqbal J, Abbasi BA, Mahmood T, Hameed S, Munir A, Kanwal S. Green synthesis and characterizations of Nickel oxide nanoparticles using leaf extract of Rhamnus virgata and their potential biological applications. Appl Organomet Chem. 2019;33(8):e4950.
14. Barzinjy, A. A., Hamad, S. M., Aydın, S., Ahmed, M. H., & Hussain, F. H. S. (2020). Green and eco-friendly synthesis of nickel oxide nanoparticles and its photocatalytic activity for methyl orange degradation. Journal of Materials Science: Materials in Electronics, 31, 11303–11316.
15. Khan, S. A., Shahid, S., Ayaz, A., Alkahtani, J., Elshikh, M. S., & Riaz, T. (2021). Phytomolecules-Coated NiO Nanoparticles Synthesis Using Abutilon indicum Leaf Extract: Antioxidant, Antibacterial, and Anticancer Activities. International journal of nanomedicine, 16, 1757–1773.
16. Gürsoy, G., Çiçek Z., Tekerek S., Kiray E., Tanriverdi A., and Çakmak E. 2024. "Synthesis of NiO Nanoparticles From Paulownia tomentosa Plant Extracts via a Green Synthesis Method and Antibacterial, Antibiofilm and Cytotoxicity Applications." Applied Organometallic Chemistry 38: e7492.
17. Angel Ezhilarasi, A., Judith Vijaya, J., Kaviyarasu, K., John Kennedy, L., Ramalingam, R. J., & Al-Lohedan, H. A. (2018). Green synthesis of NiO nanoparticles using Aegle marmelos leaf extract for the evaluation of in-vitro cytotoxicity, antibacterial and photocatalytic properties. Journal of photochemistry and photobiology. B, Biology, 180, 39–50.
18. Sukumaran, J., Priya, M., Venkatesan, R., Sathiasivan, K., Khan, M. R., & Kim, S. C. (2025). Green Synthesis of Nickel Oxide Nanoparticles Using Leaf Extract of Aegle marmelos and Their Antibacterial, Anti-Oxidant, and In Vitro Cytotoxicity Activity. Microscopy research and technique, 88(10), 2830–2842.
19. Mirza, A.U., Khan, M.S., Kareem, A. et al. Biomediated synthesis, characterization, and biological applications of nickel oxide nanoparticles derived from Toona ciliata, Ficus carica and Pinus roxburghii. Bioprocess Biosyst Eng 44, 1461–1476 (2021).
20. Ahmad B., Khan M.I., Naeem M.A., et al. Green synthesis of NiO nanoparticles using Aloe vera gel extract and evaluation of antimicrobial activity. Materials Chemistry and Physics 2022, 288, 126363.
21. Sabouri, Z., Akbari, A., Hosseini, H. A., Khatami, M., & Darroudi, M. (2021). Green-based bio-synthesis of nickel oxide nanoparticles in Arabic gum and examination of their cytotoxicity, photocatalytic and antibacterial effects. Green Chemistry Letters and Reviews, 14(2), 404–414.
22. Al-Zaqri, N., Umamakeshvari, K., Mohana, V., et al. (2022). Green synthesis of nickel oxide nanoparticles and its photocatalytic degradation and antibacterial activity. Journal of Materials Science: Materials in Electronics, 33, 11864–11880.
23. Ahghari, M. R., Soltaninejad, V., & Maleki, A. (2020). Synthesis of nickel nanoparticles by a green and convenient method as a magnetic mirror with antibacterial activities. Scientific Reports, 10, 12627
24. Srihasam S., Thyagarajan K., Korivi M., Lebaka V.R., Mallem S.P.R. Phytogenic generation of NiO nanoparticles using Stevia leaf extract and evaluation of their in-vitro antioxidant and antimicrobial properties. Biomolecules 2020, 10(1), 89.
25. Kganyago P., Mahlaule-Glory L.M., Mathipa M.M., et al. Synthesis of NiO nanoparticles via a green route using Monsonia burkeana: The physical and biological properties. Journal of Photochemistry and Photobiology B: Biology 2018, 182, 18–26.
26. Slavin, Y. N., Asnis, J., Häfeli, U. O., & Bach, H. (2017). Metal nanoparticles: understanding the mechanisms behind antibacterial activity. Journal of Nanobiotechnology, 15, 65.

27. Dizaj, S. M., Lotfipour, F., Barzegar-Jalali, M., Zarrintan, M. H., & Adibkia, K. (2014). Antimicrobial activity of the metals and metal oxide nanoparticles. Materials Science and Engineering: C, 44, 278–284.
28. Narender, S. S., Varma, V. V. S., Srikar, C. S., Ruchitha, J., Varma, P. A., & Praveen, B. V. S. (2022). Nickel oxide nanoparticles: A brief review of their synthesis, characterization, and applications. Chemical Engineering & Technology, 45, 397–409.
29. Nande A, Raut S, Michalska-Domanska M, Dhoble S.J. Green Synthesis of Nanomaterials Using Plant Extract: A Review. Current Pharmaceutical Biotechnology 22(13):1794–1811 (2021).
30. Singh, H., Desimone, M. F., Pandya, S., Jasani, S., George, N., Adnan, M., Aldarhami, A., Bazaid, A. S., & Alderhami, S. A. (2023). Revisiting the Green Synthesis of Nanoparticles: Uncovering Influences of Plant Extracts as Reducing Agents for Enhanced Synthesis Efficiency and Its Biomedical Applications. International journal of nanomedicine, 18, 4727–4750.
31. Din, M. I., Rani, A., & Ahmad, M. (2016). Recent advances in the synthesis and stabilization of nickel and nickel oxide nanoparticles: A green adeptness. International Journal of Analytical Chemistry, 2016, Article 3512145.
32. Lingaraju, K., Naika, H. R., Nagabhushana, H., Jayanna, K., Devaraja, S., & Nagaraju, G. (2020). Biosynthesis of nickel oxide nanoparticles from Euphorbia heterophylla (L.) and their biological application. Arabian Journal of Chemistry, 13(3), 4712–4719.
33. Singh, Y., Sodhi, R. S., Singh, P. P., & Kaushal, S. (2022). Biosynthesis of NiO nanoparticles using Spirogyra sp. cell-free extract and their potential biological applications. Materials Advances, 3(12), 4991–5000.
34. Panigrahy SK., Singhamahapatra A., Jena M. and Sahoo S., (2020). Green Synthesis of Metal Nanoparticles using Ocimum sanctum (Tulsi) International Journal of Pharmacy and Biological Sciences 10 (2): 338-349.
35. Fadliah, F., Raya, I., Ahmad, A., Taba, P., Burhanuddinnur, M., Gaffar, M., Putri, T. W., Nur, A., Abubakar, A. N. F., Munadi, R., Majid, A. F., Pratama, I., Yasser, M., Jarre, S., & Karim, H. (2025). Synthesis and characterization of nickel nanoparticles: Biological and photocatalytic properties. Indonesian Journal of Chemistry, 25(1).
36. Chowdhury, M. A. S., Islam, M. M., & Jamal, M. (2025). Green synthesis of nickel oxide nanoparticles using Allium cepa stalks and investigation of their antibacterial activity. Results in Chemistry, 16, 102328.
37. Feltin, N., & Zeng, G. (2020). Energy-dispersive X-ray spectroscopy (EDS). In Characterization of Nanoparticles, pp. 397–417.
38. Gryboś, J., Indyka, P., & Sojka, Z. (2021). Morphology, structure, and chemical composition: Transmission electron microscopy and elemental analysis. In Metal Oxide Nanoparticles, pp. 349-382.
39. Espenti, C. S., Rao, K. M., Rao, K. S. V. K., Mettu, M. R., & Han, S. S. (2025). Advancements in transmission and scanning electron microscopy for nanomaterials: Insights into structural, morphological, and functional characteristics. Applied Materials Today, 46, 102829.
40. Lazim, K. A., & Moghaddam, H. M. (2025). Green synthesis of nickel nanoparticles using Lawsonia inermis extract and evaluation of their effectiveness against Staphylococcus aureus. Al-Mustansiriyah Journal of Science, 36(1), 84–91.
41. Magaldi, S., Mata-Essayag, S., Hartung de Capriles, C., Pérez, C., Colella, M. T., Olaizola, C., & Ontiveros, Y. (2004). Well diffusion for antifungal susceptibility testing. International Journal of Infectious Diseases, 8(1), 39–45.
42. Balouiri, M., Sadiki, M., & Ibnsouda, S. K. (2016). Methods for in vitro evaluating antimicrobial activity: A review. Journal of Pharmaceutical Analysis, 6(2), 71–79.
43. McFarland, J. (1907). The nephelometer: an instrument for estimating the number of bacteria in suspensions used for calculating the opsonic index and for vaccines. Journal of the American Medical Association, 49(14), 1176–1178.
44. Brand-Williams, W.; Cuvelier, M. E.; Berset, C. Use of a free radical method to evaluate antioxidant activity. LWT—Food Science and Technology 1995, 28, 25–30.
45. Kareem, M. M., Babu, H., & Lakshmi, G. V. (2023). Anticancer, antibacterial, antioxidant, and photo-catalytic activities of eco-friendly synthesized Ni nanoparticles. Inorganic Chemistry Communications, 148, 110274.
46. Bollinger, J.-C., Lima, E. C., Mouni, L., Salvestrini, S., & Tran, H. N. (2025). Molecular properties of methylene blue, a common probe in sorption and degradation studies: A review. Environmental Chemistry Letters, 23, 1403–1424
47. Din, M. I., Khalid, R., Najeeb, J., & Hussain, Z. (2021). Fundamentals and photocatalysis of methylene blue dye using various nanocatalytic assemblies—A critical review. Journal of Cleaner Production, 298, 126567.
48. Din, M. I., Tariq, M., Hussain, Z., & Khalid, R. (2020). Single step green synthesis of nickel and nickel oxide nanoparticles from Hordeum vulgare for photocatalytic degradation of methylene blue dye. Inorganic and Nano-Metal Chemistry, 50(4), 292–297.
49. Pandian, C. J., Palanivel, R., & Dhananasekaran, S. (2015). Green synthesis of nickel nanoparticles using Ocimum sanctum and their application in dye and pollutant adsorption. Chinese Journal of Chemical Engineering, 23(8), 1307–1315.
50. Elango, G., Roopan, S. M., Dhamodaran, K. I., Elumalai, K., Al-Dhabi, N. A., & Arasu, M. V. (2016). Spectroscopic investigation of biosynthesized nickel nanoparticles and its larvicidal, pesticidal activities. Journal of Photochemistry and Photobiology B: Biology, 162, 162–167. https://doi.org/10.1016/j.jphotobiol.2016.06.045
51. Huang, Y., Zhu, C., Xie, R., & Ni, M. (2021). Green synthesis of nickel nanoparticles using Fumaria officinalis as a novel chemotherapeutic drug for the treatment of ovarian cancer. Journal of Experimental Nanoscience, 16(1), 368–381.
52. Kumar, N., Singh, A., & Devra, V. (2025). Experimental investigation on plant extract-induced biosynthesis of nickel nanoparticles. Next Nanotechnology, 7, 100104. https://doi.org/10.1016/j.nxnano.2024.100104
53. Gao, Y., Zhao, J., Zhou, B., Zhu, Y., & Wang, Z. (2010). Aqueous synthesis of flower-like nickel nanostructures under the induction of magnetic field. Colloids and Surfaces A: Physicochemical and Engineering Aspects, 368(1–3), 137–141. https://doi.org/10.1016/j.colsurfa.2010.07.028

54. Chaudhary, R. G., Tanna, J. A., Gandhare, N. V., Rai, A. R., & Juneja, H. D. (2015). Synthesis of nickel nanoparticles: Microscopic investigation, an efficient catalyst and effective antibacterial activity. Advanced Materials Letters, 6(11), 990–998.
55. Wang, C., Zong, L., Pan, Y., Liu, Q., Wang, J., & Jian, X. (2021). Preparation and characterization of branch-like heteroatoms-doped Ni@C nanofibers for high-performance microwave absorption with thin thickness. Composites Science and Technology, 216, 109054. https://doi.org/10.1016/j.compscitech.2021.109054.
56. Yuan, C., Jiang, B., Xu, X., Wan, Y., Wang, L., & Chen, J. (2022). Anti-human ovarian cancer and cytotoxicity effects of nickel nanoparticles green-synthesized by Alhagi maurorum leaf aqueous extract. Journal of Experimental Nanoscience, 17(1), 113–125. https://doi.org/10.1080/17458080.2021.2011860.
57. Kondak, S., Kondak, D., Kabadayi, O., Erdei, L., Rónavári, A., Kónya, Z., Galbács, G., & Kolbert, Z. (2024). Current insights into the green synthesis, in planta characterization and phytoeffects of nickel nanoparticles and their agricultural implications. Environmental Research, 260, 119665
58. Jayamani, R., Krishnaveni, R., Sethupathi, M., Dixit, S., Devanesan, S., Shanmugaraj, K., & Palanisamy, G. (2025). Biosynthesis of nickel nanoparticles using aqueous Aerva lanata extract and their utilization in antimicrobial activity. BioMetals, 40(11), e70364.
59. Balto, H., Amina, M., Bhat, R. S., Al-Yousef, H. M., Auda, S. H., & Elansary, A. (2023). Green Synthesis of Nickel Nanoparticles Using Salvadora persica and Their Application in Antimicrobial Activity against Oral Microbes. Microbiology Research, 14(4), 1879-1893.
60. Clinical and Laboratory Standards Institute. (2024). Performance standards for antimicrobial disk susceptibility tests (14th ed.; CLSI standard M02). Clinical and Laboratory Standards Institute. CLSI M02 standard
61. Pisoschi, A. M., & Pop, A. (2015). The role of antioxidants in the chemistry of oxidative stress: A review. European Journal of Medicinal Chemistry, 97, 55–74.
62. Behera, A., Sirivela, S., Ryntathiang, I., et al. (2026). Biosynthesis of nickel nanoparticles using Shorea robusta extract and evaluation of their antioxidant, antibacterial, anti-inflammatory, wound healing, and environmental applications. Discover Chemistry, 3, 314
63. Girotto, G. Z., Thill, A. S., Matte, L. P., Vogt, M. A. H., Machado, T. V., Dick, L. F. P., Mesquita, F., & Bernardi, F. (2022). Ni/$SrTiO_3$ nanoparticles for photodegradation of methylene blue. ACS Applied Nano Materials, 5(9), 13295–13307.